Robustness Analysis of Helicopter Ground Resonance with Parametric Uncertainties in Blade Properties

Leonardo Sanches[1] and Daniel Alazard[2]
Université Toulouse, DMIA, ISAE, 10 av. Édouard Belin, 31055 Toulouse, France

Guilhem Michon[3]
Université Toulouse, ICA, ISAE, 10 av. Édouard Belin, 31055 Toulouse, France

Alain Berlioz[4]
Université Toulouse, ICA, UPS, 118 route de Narbonne 31062 Toulouse, France

This paper presents a stability robustness analysis of the helicopter ground resonance phenomenon. By using the lifting procedure, the uncertain Linear Time-Periodic (LTP) model of the helicopter is transformed into an augmented uncertain Linear-Time-Invariant (LTI) model that allows the application of μ-analysis tools. The lifting procedure involves a periodic switching LTI piecewise model computed using oversampling of the system period. The representativeness of the lifted model for various oversampling period values and discretization methods is discussed and compared with a Floquet analysis for several parametric configurations. A μ-analysis is then applied to find the worst case parametric configuration for a given rotor angular rate. The parametric uncertainties taken into account are the dynamic characteristics (stiffness and damping) of each blade hinge. A significant advantage of the proposed approach is that it enables performing ground resonance analysis for a rotor with dissimilar blade properties due to aging effects. Considering uncertainties on the four blade hinge stiff-

---

[1] PhD. student.
[2] Professor, (ISAE/DMIA).
[3] Associate Professor, (ISAE/DMSM).
[4] Professor, (UPS).

nesses and damping factors, the μ-analysis performed on the lifted model leads to the conclusion that the worst case for degraded rotor stability corresponds to the symmetric perturbation of all the blades.

Nomenclature

$\mathbf{A}(t)$, $\mathbf{B}(t)$, $\mathbf{C}(t)$, $\mathbf{D}(t)$	=	continuous-time state-space matrices
$\underline{\mathbf{A_c}}$, $\underline{\mathbf{B_c}}$, $\underline{\mathbf{C_c}}$, $\underline{\mathbf{D_c}}$	=	state-space matrices of the continuous-time lifted model
$\mathbf{A_d}(k)$, $\mathbf{B_d}(k)$, $\mathbf{C_d}(k)$, $\mathbf{D_d}(k)$	=	discrete-time state-space matrices
$\underline{\mathbf{A_d}}$, $\underline{\mathbf{B_d}}$, $\underline{\mathbf{C_d}}$, $\underline{\mathbf{D_d}}$	=	state-space matrices of the discrete-time lifted model
a	=	rotor eccentricity (m)
b	=	blade equivalent length (m)
C_X, C_Y	=	fuselage damping factors in x and y directions (Ns/m)
$C_{b\,k}$	=	k-th blade hinge damping factor (Nms/rad)
$\mathbf{F}_{ext}$	=	normalized external force vector
h	=	oversampling period (s)
$\mathbb{O}_{n\times m}$	=	$n \times m$ null matrix
$\mathbb{I}_n$	=	$n \times n$ identity matrix
$I_{Zb\,k}$	=	k-th blade lag inertia ($\mathrm{kg\,m^2}$)
$K_{b\,k}$	=	k-th blade hinge stiffness ($\mathrm{N\,m\,rad^{-1}}$)
K_{f_X}, K_{f_Y}	=	fuselage longitudinal and lateral stiffnesses ($\mathrm{N\,m^{-1}}$)
$\mathbf{M}, \mathbf{K}, \mathbf{D}$	=	mass, stiffness and damping matrices
m_f, $m_{b\,k}$	=	fuselage and k-th blade masses (kg)
n	=	system order (integer)
n_h	=	number of over-samples in one period (integer)
N_b	=	number of blades (integer)
p	=	number of uncertain parameters
$\mathbf{q}$	=	vector of degrees of freedom

$r_{a\,k}$ $= \sqrt{a\, r_{b\,k}}$

$r_{b\,k}$ = k-th blade static moment to total inertia ratio (m^{-1})

$r_{c\,k}$ = k-th blade damping factor to total inertia ratio (s^{-1})

$r_{c\,X}$, $r_{c\,Y}$ = fuselage damping factor to total mass ratios, (s^{-1})

$r_{m\,k}$ = k-th blade static moment to total mass ratio (m)

$\mathbf{R}$ = monodromy matrix

t = time (s)

T = period of the Linear-Time-Periodic (LTP) system (s)

$\mathbf{V}$ = permutation matrix

$\mathbf{x}$,$\mathbf{w}$,$\mathbf{z}$ = state, input and output vectors

$x\,(t)$, $y\,(t)$ = fuselage longitudinal and lateral position (m)

x_{bk}, y_{bk} = k-th blade positions (m)

$(x,\, y,\, z)$ = frame attached to the rotor hub

$(X_0,\, Y_0,\, Z_0)$ = inertial frame

$\mathbf{\Delta}$ = uncertainty matrix

μ = structured singular value

$\varphi_k\,(t)$ = $k-th$ blade lead-lag angle (rad)

Ω = rotor angular velocity ($\mathrm{rad\,s}^{-1}$)

ζ_k = k-th blade azimuth angle (rad)

$\omega_{b\,k}$ = k-th blade cantilevered frequency ($\mathrm{rad\,s}^{-1}$)

ω_x, ω_y = cantilevered fuselage frequencies ($\mathrm{rad\,s}^{-1}$)

$\mathbf{\Phi}(t, t_0)$ = transition matrix

Subscripts and exponents

a = approximated

c = continuous

d = discrete

p = perturbed

$\mathbf{T}$ = transposed

Accents

$\dot{\mathbf{x}}$	= time-domain derivative of $\mathbf{x}$
$\widetilde{\mathbf{w}}$	= $\mathbf{w}$ permuted
$\underline{\mathbf{w}}$	= $\mathbf{w}$ augmented

I. Introduction

Helicopter ground resonance is a dynamical phenomenon that has attracted much attention of from researchers over the last five decades, particularly for rotors with hinged blades and a shift (offset) between the hinge axis and the main rotor axis. The prediction of critical rotor velocities at which the phenomenon occurs was first studied by Coleman and Feingold [1] for helicopters with rotors with identical blade properties. The equations of motions were simplified [2] by eliminating their periodical characteristic and Linear Time Invariant (LTI) stability analysis was performed easily.

Major contributions to understanding this phenomenon in hingeless and bearingless rotors have been made since[3, 4]. Criteria for determining the dimension of viscous dampers have been established and the design of passive control systems has been studied in order to dissipate energies and avoid unstable motions [5–7]. Semi-active and active control solutions using the pitch angle of each blade have also been proposed to reduce vibrations [8, 9].

However, the effects of aging on various mechanical elements can induce unbalanced parametric variations from one blade to another and compromise the rotor's nominal behavior, leading to dangerous conditions in extreme cases. In the field of aeronautics such situations must be mastered to reduce not only human risk but also maintenance costs. Therefore analysis tools for rotors with dissimilar blades are required to assess ground resonance instability.

When considering blades with different mechanical properties, the simplifications made by Coleman are no longer valid and Floquet theory has been used to study the stability of time-periodic equations of motion [10, 11]. Predicting the ground resonance phenomenon for a wide range of dissimilar blade configurations means analyzing each point individually on a grid of parametric space,

generating high computational costs. Furthermore, there is no guarantee that parametric gridding includes the worst-case parametric configuration.

On the other hand, the stability and performance robustness of linear time-invariant (LTI) systems under structural uncertainties have been analyzed by using the standard μ-analysis method and efficient tools are now available [12][1] [2]. In [13], the parametric robustness analysis of LTP systems is considered using a truncated point mapping technique and μ-analysis. The continuous-time LTP model is transformed into a discrete-time LTI model and the size of the uncertainty block is increased according to the truncation order. Additional uncertainties are taken into account to handle this truncation error but introduce conservatism. In [14–18], symbolic methods (e.g., the multiple scale and harmonic balance methods) are used to analyze helicopter ground resonance by considering mechanical nonlinearities. However, the influence of dissimilarities from one blade to the other in such systems was not studied. The robustness of uncertain polytopic discrete-time periodic systems was considered in [19] from the standpoint of periodic state-feedback design. The robustness analysis of ground resonance stability has been addressed more recently in [20]. The authors considered complex uncertainties embedding uncertainties on the stiffness and damping ratio of lead-lag dampers, but under the assumption that these dampers are identical from one blade to the other. However, the direct analysis of ground resonance stability for asymmetric rotor properties was dealt with unsatisfactorily.

Recently, the problem of robustness analysis of linear time periodic (LTP) dynamical systems [21] under structured LTI uncertainties was solved [22, 23], by combining Floquet theory with the lifting technique [24–26]. The original uncertain LTP system was cast in the form of a Linear Fractional Transformation (LFT) using discretization on an oversampling of the system period in order to use μ-analysis methods. The time-lifted LFT model involves an uncertainty structure with highly-repeated parameters which can raise problems for performing μ-analyses. In order to reduce the size of the uncertainty block and the associated computational burden of μ-analyses,

---

[1] Ferreres, G. and Biannic, J.-M., "The Skew Mu Toolbox", `http://www.onera.fr/staff-en/jean-marc-biannic/`.
[2] Peaucelle, D., "RoMulOC: Robust Multi-Objective Control Toolbox",`http://spiderman-2.laas.fr/OLOCEP/romuloc/index.html`.

the representativeness of the (lifted) LFT model for various oversampling period values and three discretization methods (zero-order hold (zoh), first-order hold (foh) and Tustin method [27, 28]) is discussed in comparison with Floquet analysis for several parametric configurations. A general MATLAB® function was developed to implement this lifting procedure to any LTP model.

The contributions of this paper are:

- to provide practical and low CPU time-consuming tools allowing the application of μ-analysis to LTP systems and
- to analyze helicopter ground resonance stability under parametric uncertainties using these tools and μ-analysis.

The example studied corresponds to independent uncertainties on (lead-lag) blade hinge stiffnesses and damping factors. The method proposed can be applied to any kind of parametric uncertainty but the result of analysis on the sensitivity to blade hinge stiffnesses (damping) is worth mentioning. It is shown that the worst case parametric configuration corresponds to an identical variation of each stiffness (damping), i.e. a rotor with identical blade dynamic properties.

Section 2 describes the lifting procedure for an uncertain LTP system with particular emphasis given to the discretization method. In section 3, the dynamic model used to study the ground resonance phenomenon is derived, the lifting procedure is validated and the results of stability analysis using the method proposed and μ-analysis are presented. Section 4 presents the conclusions.

II. Robustness Analysis of LTP Systems

A. General background

Consider the uncertain LTP system $\mathcal{S}(\mathbf{\Delta})$ defined by an LFT representation $\mathcal{M}(s,t) - \mathbf{\Delta}$:

$$\mathcal{M}(s,t): \begin{cases} \dot{\mathbf{x}}(t) = \mathbf{A}(t)\,\mathbf{x}(t) + \mathbf{B}(t)\,\mathbf{w}(t) \\ \mathbf{z}(t) = \mathbf{C}(t)\,\mathbf{x}(t) + \mathbf{D}(t)\,\mathbf{w}(t) \end{cases} \quad \text{with:} \quad \mathbf{w}(t) = \mathbf{\Delta}\,\mathbf{z}(t) \tag{1}$$

where $\mathbf{x}(t) \in \mathbb{R}^n$ is the state vector, $\mathbf{w}(t)$ and $\mathbf{z}(t)$ are input and output vectors of the LFT. The structured uncertainty matrix $\mathbf{\Delta}$ is a $p \times p$ diagonal matrix of unknown but bounded real parameters:

$$\mathbf{\Delta} = \mathrm{diag}\,[\delta_1, \delta_2, \ldots, \delta_p] \tag{2}$$

Matrices $\mathbf{A}(t)$, $\mathbf{B}(t)$, $\mathbf{C}(t)$ and $\mathbf{D}(t)$ are real, piecewise continuous and periodic with a period T,

$$\mathbf{A}(t+T) = \mathbf{A}(t),\ \mathbf{B}(t+T) = \mathbf{B}(t),\ \mathbf{C}(t+T) = \mathbf{C}(t),\ \mathbf{D}(t+T) = \mathbf{D}(t)\ . \tag{3}$$

The closed-loop LFT representation is

$$\dot{\mathbf{x}}(t) = \left(\mathbf{A}(t) + \mathbf{B}(t)\boldsymbol{\Delta}(\mathbb{I}_n - \mathbf{D}(t)\boldsymbol{\Delta})^{-1}\mathbf{C}(t)\right)\ \mathbf{x}(t) = \mathbf{A_p}(t, \boldsymbol{\Delta})\,\mathbf{x}(t) \tag{4}$$

where the matrix $\mathbf{A_p}(t, \boldsymbol{\Delta})$ is also T-periodic.

The nominal system ($\boldsymbol{\Delta} = 0$) is assumed to be stable. The parametric robustness analysis consists in finding the smallest uncertainty $\boldsymbol{\Delta}_{\mathbf{worst}}$ matrix which makes the closed-loop system (4) unstable.

Floquet theory [29, 30] can be used to analyze the stability for a particular value of $\boldsymbol{\Delta}$. Considering the transition matrix $\boldsymbol{\Phi}(t, t_0, \boldsymbol{\Delta})$ associated with the closed-loop system (4), the stability analysis is then characterized by the **monodromy matrix** $\mathbf{R}(t_0, \boldsymbol{\Delta})$ defined as the transition matrix over one period:

$$\mathbf{R}(t_0, \boldsymbol{\Delta}) = \boldsymbol{\Phi}(t_0 + T, t_0, \boldsymbol{\Delta})\ . \tag{5}$$

Without loss of generality, it can be assumed that $t_0 = 0$.

Then, the system (4) is exponentially stable if and only if $\mathbf{R}(\boldsymbol{\Delta}) = \mathbf{R}(t_0 = 0, \boldsymbol{\Delta})$ is Schur, i.e., all the eigenvalues of $\mathbf{R}(\boldsymbol{\Delta})$, also called **characteristic multipliers**: $\lambda_i(\boldsymbol{\Delta}) \quad i = 1, 2, \ldots, n$, have a magnitude less than one.

In most practical cases matrix $\mathbf{R}(\boldsymbol{\Delta})$ cannot be determined analytically. Nevertheless, $\mathbf{R}(\boldsymbol{\Delta})$ can be approximated by assuming that the system in Eq.(4) can be represented in the form of a periodic linear switched system defined by [29]:

$$\dot{\mathbf{x}}(t) = \mathbf{A_p}(kh, \boldsymbol{\Delta})\mathbf{x}(t) \tag{6}$$

$$\forall\ t \in [lT + kh,\ lT + (k+1)h[, \quad l = 0, 1, 2, \ldots, \quad k = 0, 1, 2, \ldots\ n_h - 1$$

where $h = \frac{T}{n_h}$ is the oversampling period and n_h is a positive integer. That is to say the system is assumed to be LTI during the oversampling period h.

The LFT representation of the switched system (6) is:

$$\mathcal{M}(s,kh): \begin{cases} \dot{\mathbf{x}}(t) = \mathbf{A}(kh)\,\mathbf{x}(t) + \mathbf{B}(kh)\,\mathbf{w}(t) \\ \mathbf{z}(t) = \mathbf{C}(kh)\,\mathbf{x}(t) + \mathbf{D}(kh)\,\mathbf{w}(t) \end{cases} \tag{7}$$

$$\text{with:} \quad \mathbf{w}(t) = \mathbf{\Delta}\,\mathbf{z}(t)$$

$$\forall t \in [kh + lT,\ (k+1) + lT[, \quad l = 0,1,2,\ldots, \quad k = 0,1,\ldots,n_h - 1$$

and can be represented by the augmented $\underline{\mathcal{M}}(s) - \underline{\mathbf{\Delta}}$ interconnection shown in Figure 1. This LFT involves n_h blocks $\mathbf{\Delta}$ "packed" in a $p\,n_h \times p\,n_h$ augmented uncertainty block $\underline{\mathbf{\Delta}}$.

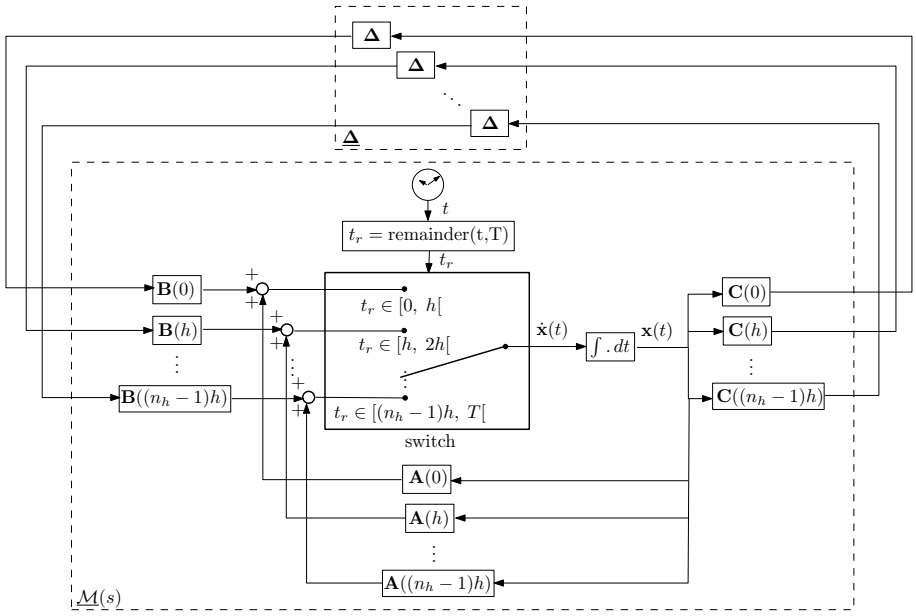

Figure 1: Sketch of the n_h LTI models switched over one period T in positive feedback with the augmented uncertainty block $\underline{\mathbf{\Delta}}$ (direct feed-through matrices are omitted for legibility).

The integration over one period of the n_h switched LTI systems allows approximating the monodromy matrix $\mathbf{R}(\mathbf{\Delta})$ by $\mathbf{R_a}(\mathbf{\Delta})$:

$$\mathbf{R}(\mathbf{\Delta}) \approx \mathbf{R_a}(\mathbf{\Delta}) = \prod_{k=0}^{n_h-1} \mathrm{e}^{\mathbf{A_p}(kh,\mathbf{\Delta})h} = \mathrm{e}^{\mathbf{A_p}((n_h-1)h,\mathbf{\Delta})h} \ldots \mathrm{e}^{\mathbf{A_p}(h,\mathbf{\Delta})h} \mathrm{e}^{\mathbf{A_p}(0,\mathbf{\Delta})h}\,. \tag{8}$$

Thus computation of the monodromy matrix on a p-dimension parametric space gridding would be too CPU time-consuming to characterize the stability in the whole parameter space. Eq.(8) will be used to validate the lifting procedure proposed in the next section for several representative

parametric configurations and for the worst-case parametric configuration provided by the μ-analysis on the lifted model (section III).

B. The lifting procedure

The lifting method is performed as follows [22]. Initially, the n_h continuous-time LTI systems $\mathcal{M}(s, kh)$ ($k = 0, 1, \cdots, n_h - 1$) defined by Eq. (7) and represented in Figure 1 are discretized with a sampling period h, as discussed in section II C. The resulting discrete-time periodic system is:

$$\mathcal{M}_d(\mathrm{z}, k) : \begin{cases} \mathbf{x_d}(k+1) &= \mathbf{A_d}(k)\,\mathbf{x_d}(k) + \mathbf{B_d}(k)\,\mathbf{w_d}(k) \\ \mathbf{z_d}(k) &= \mathbf{C_d}(k)\,\mathbf{x_d}(k) + \mathbf{D_d}(k)\,\mathbf{w_d}(k) \end{cases} \quad \text{with:} \quad \mathbf{w_d}(k) = \mathbf{\Delta}\,\mathbf{z_d}(k)\ . \tag{9}$$

Matrices $\mathbf{A_d}(k)$, $\mathbf{B_d}(k)$, $\mathbf{C_d}(k)$ and $\mathbf{D_d}(k)$ depend on the discretization method and are n_h-periodic:

$$\mathbf{A_d}(k+n_h) = \mathbf{A_d}(k),\ \mathbf{B_d}(k+n_h) = \mathbf{B_d}(k),\ \mathbf{C_d}(k+n_h) = \mathbf{C_d}(k),\ \mathbf{D_d}(k+n_h) = \mathbf{D_d}(k)\ . \tag{10}$$

In the second step, the system (9) is integrated over one period n_h. The final discrete-time-invariant LFT model $\underline{\widetilde{\mathcal{M}}}_d(\mathrm{z}) - \underline{\widetilde{\mathbf{\Delta}}}$ ("lifted" model) is:

$$\underline{\widetilde{\mathcal{M}}}_d(\mathrm{z}) : \begin{cases} \mathbf{x_d}(k+n_h) &= \underline{\mathbf{A_d}}\,\mathbf{x_d}(k) + \underline{\mathbf{B_d}}\mathbf{V^T}\,\underline{\widetilde{\mathbf{w}}_\mathbf{d}}(k) \\ \underline{\widetilde{\mathbf{z}}_\mathbf{d}}(k) &= \mathbf{V}\underline{\mathbf{C_d}}\,\mathbf{x_d}(k) + \mathbf{V}\underline{\mathbf{D_d}}\mathbf{V^T}\,\underline{\widetilde{\mathbf{w}}_\mathbf{d}}(k) \end{cases} \quad \text{with:} \quad \underline{\widetilde{\mathbf{w}}_\mathbf{d}}(k) = \underline{\widetilde{\mathbf{\Delta}}}\,\underline{\widetilde{\mathbf{z}}_\mathbf{d}}(k) \tag{11}$$

where: $\underline{\widetilde{\mathbf{\Delta}}} = \mathrm{diag}\,[\delta_1 \mathbb{I}_{n_h}, \delta_2 \mathbb{I}_{n_h}, \ldots \delta_p \mathbb{I}_{n_h}]$. Matrices ($\underline{\mathbf{A_d}}$, $\underline{\mathbf{B_d}}$, $\underline{\mathbf{C_d}}$, $\underline{\mathbf{D_d}}$), the re-ordering matrix $\mathbf{V}$, augmented input and output vectors $\underline{\widetilde{\mathbf{w}}_\mathbf{d}}(k)$ and $\underline{\widetilde{\mathbf{z}}_\mathbf{d}}(k)$ are detailed in Appendix A.

The third step uses an inverse Tustin transform to convert the system $\underline{\widetilde{\mathcal{M}}}_d(\mathrm{z})$ (Eq. 11) back to the continuous-time domain in order to apply μ-analysis tools available only in continuous-time. Since the μ-analysis is performed in the frequency domain, the Tustin transform (with a sampling period equal to T) is selected here for its property of preserving the input-output frequency-domain response [27]. The final continuous-time-invariant LFT model $\underline{\widetilde{\mathcal{M}}}_c(s) - \underline{\widetilde{\mathbf{\Delta}}}$ is

$$\underline{\widetilde{\mathcal{M}}}_c(s) : \begin{cases} \dot{\mathbf{x_c}}(t) &= \underline{\mathbf{A_c}}\,\mathbf{x_c}(t) + \underline{\mathbf{B_c}}\,\underline{\widetilde{\mathbf{w}}_\mathbf{c}}(t) \\ \underline{\widetilde{\mathbf{z}}_\mathbf{c}}(t) &= \underline{\mathbf{C_c}}\,\mathbf{x_c}(t) + \underline{\mathbf{D_c}}\,\underline{\widetilde{\mathbf{w}}_\mathbf{c}}(t) \end{cases} \quad \text{with:} \quad \underline{\widetilde{\mathbf{w}}_\mathbf{c}}(t) = \underline{\widetilde{\mathbf{\Delta}}}\,\underline{\widetilde{\mathbf{z}}_\mathbf{c}}(t) \tag{12}$$

where:

- $\underline{\mathbf{A_c}} = \frac{2}{T}(\mathbb{I}_n + \underline{\mathbf{A_d}})^{-1}(\underline{\mathbf{A_d}} - \mathbb{I}_n)$
- $\underline{\mathbf{B_c}} = \frac{2}{T}(\mathbb{I}_n + \underline{\mathbf{A_d}})^{-1}\underline{\mathbf{B_d}}\mathbf{V^T}$
- $\underline{\mathbf{C_c}} = 2\mathbf{V}\underline{\mathbf{C_d}}(\mathbb{I}_n + \underline{\mathbf{A_d}})^{-1}$
- $\underline{\mathbf{D_c}} = \mathbf{V}\underline{\mathbf{D_d}}\mathbf{V^T} - \mathbf{V}\underline{\mathbf{C_d}}(\mathbb{I}_n + \underline{\mathbf{A_d}})^{-1}\underline{\mathbf{B_d}}\mathbf{V^T}$

The original LTP system $\mathcal{S}(\boldsymbol{\Delta})$ in Eq.(1) is now in the standard continuous-time LFT form $\widetilde{\underline{\mathcal{M}}}_c(s) - \widetilde{\underline{\boldsymbol{\Delta}}}$, as given in Eq.(12). In the next section, the lifting procedure[3]. is applied to the parametric robustness analysis of the ground resonance phenomenon.

C. Discretization methods

From the stability analysis accuracy point of view, errors in the evaluation of the perturbed monodromy matrix $\mathbf{R_a}(\boldsymbol{\Delta})$ and its characteristic multipliers can only be introduced in the first step (discretization). The approach was to re-use the discretization methods commonly used in the field of automatic control [27]: (i) impulse invariance, (ii) zero-order hold, (iii) first-order hold, (iv) Tustin transformation, (v) matched pole-zero. The impulse invariance and matched pole-zero methods are not considered since the impulse invariance method cannot handle systems with direct feed-through and the matched pole-zero method works only for single-input single-output systems. The three remaining methods are compared here from the angle of monodromy matrix $\mathbf{R_a}(\boldsymbol{\Delta})$ approximation.

For $k = 0, \cdots, n_h$ the closed-loop LFT representation (9) is:

$$\begin{aligned}\mathbf{x_d}(k+1) &= \left(\mathbf{A_d}(k) + \mathbf{B_d}(k)\boldsymbol{\Delta}(\mathbb{I}_n - \mathbf{D_d}(k)\boldsymbol{\Delta})^{-1}\mathbf{C_d}(k)\right)\,\mathbf{x_d}(k) \\ &= \mathbf{A_{d\,p}}(k, \boldsymbol{\Delta})\,\mathbf{x_d}(k)\end{aligned} \tag{13}$$

and by integration over one period n_h, the closed-loop lifted LFT (11) can be expressed as:

$$\mathbf{x_d}(k + n_h) = \prod_{k=0}^{n_h-1} \mathbf{A_{d\,p}}(k, \boldsymbol{\Delta})\,\mathbf{x_d}(k)\ . \tag{14}$$

---

[3] The whole procedure for converting an LTP system into a continuous-time lifted system is embedded in a MATLAB® function `ltp2lti.m` which can be downloaded from `http://personnel.isae.fr/daniel-alazard/matlab-packages/lifting-procedure-for-linear-time.html`. The package also contains a tutorial on the Mathieu equation.

The objective is to approximate the uncertain monodromy matrix for any value of $\boldsymbol{\Delta}$:

$$\mathbf{R_a}(\boldsymbol{\Delta}) = \prod_{k=0}^{n_h-1} \mathrm{e}^{\mathbf{A_p}(kh,\boldsymbol{\Delta})h} \approx \prod_{k=0}^{n_h-1} \mathbf{A_{dp}}(k,\boldsymbol{\Delta})\,. \tag{15}$$

Therefore, for all k, matrices $\mathrm{e}^{\mathbf{A_p}(kh,\boldsymbol{\Delta})h}$ and $\mathbf{A_{dp}}(k,\boldsymbol{\Delta})$ must be compared for the various discretization methods. This problem of continuous-time LFT discretization was first addressed in [31]. The discretization error according to various methods is also discussed in-depth [32, 33] in the more general framework of the Linear Parameter-Varying (LPV) system where the bounds on the discretization error are proposed in terms of approximating the state or output evolution. Here, we focus on the approximation error on the uncertain transition matrix $\mathrm{e}^{\mathbf{A_p}(kh,\boldsymbol{\Delta})h}$.

A third order Taylor expansion in h of $\mathrm{e}^{\mathbf{A_p}(kh,\boldsymbol{\Delta})h}$ leads to (kh is omitted for brevity)

$$\mathrm{e}^{\mathbf{A_p}(\boldsymbol{\Delta})h} \approx \mathbb{I}_n + (\mathbf{A}+\boldsymbol{\Delta}_\mathbf{A})h + (\mathbf{A}+\boldsymbol{\Delta}_\mathbf{A})^2\frac{h^2}{2} + (\mathbf{A}+\boldsymbol{\Delta}_\mathbf{A})^3\frac{h^3}{6}\,. \tag{16}$$

with $\boldsymbol{\Delta}_\mathbf{A} = \mathbf{B}\boldsymbol{\Delta}(\mathbb{I}_n - \mathbf{D}\boldsymbol{\Delta})^{-1}\mathbf{C}$.

The expressions of $\mathbf{A_d}(k)$, $\mathbf{B_d}(k)$, $\mathbf{C_d}(k)$, $\mathbf{D_d}(k)$ from $\mathbf{A}(kh)$, $\mathbf{B}(kh)$, $\mathbf{C}(kh)$, $\mathbf{D}(kh)$ and h, the mapping between discrete-time state $\mathbf{x_d}(k)$ and continuous-time state $\mathbf{x}(kh)$ and input $\mathbf{w}(kh)$, and the third order expansion of $\mathbf{A_d}(k,\boldsymbol{\Delta})$ are described below for the three discretization methods (k and kh are omitted for brevity):

- **Zero order hold (zoh) method** [28]: the input $\mathbf{w}(t)$ of system $\mathcal{M}(s,kh)$ is assumed to be constant over the oversampling period h:

  $$\mathbf{w}(t) = \mathbf{w_d}(k), \quad \forall\, t \in [kh,\ (k+1)h[.$$

  Then

  $$\mathbf{A_d} = \mathrm{e}^{\mathbf{A}\,h} \tag{17a}$$

  $$\mathbf{B_d} = \mathbf{A}^{-1}\left(\mathrm{e}^{\mathbf{A}\,h} - \mathbb{I_n}\right)\mathbf{B} \tag{17b}$$

  $$\mathbf{C_d} = \mathbf{C} \tag{17c}$$

  $$\mathbf{D_d} = \mathbf{D} \tag{17d}$$

  associated with the state $\mathbf{x_d}(k) = \mathbf{x}(kh)$ and

  $$\mathbf{A_{dp}}(\boldsymbol{\Delta}) \approx \mathbb{I}_n + (\mathbf{A}+\boldsymbol{\Delta}_\mathbf{A})h + \mathbf{A}(\mathbf{A}+\boldsymbol{\Delta}_\mathbf{A})\frac{h^2}{2} + \mathbf{A}^2(\mathbf{A}+\boldsymbol{\Delta}_\mathbf{A})\frac{h^3}{6}\,. \tag{18}$$

- **First order hold (foh) method**: the input $\mathbf{w}(t)$ of system $\mathcal{M}(s, kh)$ is assumed to be linear between two consecutive over-samples:

$$\mathbf{w}(t) = \mathbf{w_d}(k) + \frac{t-kh}{h}(\mathbf{w_d}(k+1) - \mathbf{w_d}(k)), \quad \forall\, t \in [kh,\ (k+1)h[.$$

Thus

$$\mathbf{A_d} = \mathrm{e}^{\mathbf{A}\,h} \tag{19a}$$

$$\mathbf{B_d} = \frac{1}{h}\mathbf{A}^{-1}\left(\mathrm{e}^{\mathbf{A}\,h} - \mathbb{I}_\mathbf{n}\right)\mathbf{B} \tag{19b}$$

$$\mathbf{C_d} = \mathbf{C}\mathbf{A}^{-1}\left(\mathrm{e}^{\mathbf{A}\,h} - \mathbb{I}_\mathbf{n}\right) \tag{19c}$$

$$\mathbf{D_d} = \mathbf{D} + \frac{1}{h}\mathbf{C}\mathbf{A}^{-1}\left(\mathrm{e}^{\mathbf{A}\,h} - \mathbb{I}_\mathbf{n} - \mathbf{A}\,h\right)\mathbf{A}^{-1}\mathbf{B} \tag{19d}$$

associated with state $\mathbf{x_d}(k) = (\mathrm{e}^{\mathbf{A}\,h} - \mathbb{I}_\mathbf{n})^{-1}(\mathbf{A}\mathbf{x}(kh) + \mathbf{B}\mathbf{w}(kh)) - \frac{1}{h}\mathbf{A}^{-1}\mathbf{B}\mathbf{w}(kh)$ and

$$\mathbf{A_{d\,p}}(\boldsymbol{\Delta}) \approx \mathbb{I}_n + (\mathbf{A}+\boldsymbol{\Delta_A})h + (\mathbf{A}+\boldsymbol{\Delta_A})^2\frac{h^2}{2} + (\mathbf{A}+\boldsymbol{\Delta_A})^3\frac{h^3}{6} + (\mathbf{A}+\boldsymbol{\Delta_A})\boldsymbol{\Delta_A}(\mathbf{A}+\boldsymbol{\Delta_A})\frac{h^3}{12}\ . \tag{20}$$

- **Tustin method** [27]: the continuous-time integration presented in Figure 1 is approximated by a numerical integration using the trapezoidal rule:

$$\mathbf{x}((k+1)h) = \mathbf{x}(kh) + \frac{h}{2}\left(\dot{\mathbf{x}}((k+1)h) + \dot{\mathbf{x}}(kh)\right)\ .$$

Then, with $\mathbf{w_d}(k) = \mathbf{w}(kh)$,

$$\mathbf{A_d} = (\mathbb{I}_n + \frac{h}{2}\mathbf{A})(\mathbb{I}_n - \frac{h}{2}\mathbf{A})^{-1} \tag{21a}$$

$$\mathbf{B_d} = h(\mathbb{I}_n - \frac{h}{2}\mathbf{A})^{-1}\mathbf{B}(kh) \tag{21b}$$

$$\mathbf{C_d} = \mathbf{C}(\mathbb{I}_n - \frac{h}{2}\mathbf{A})^{-1} \tag{21c}$$

$$\mathbf{D_d} = \mathbf{D} + \frac{h}{2}\mathbf{C}(\mathbb{I}_n - \frac{h}{2}\mathbf{A})^{-1}\mathbf{B} \tag{21d}$$

associated with state $\mathbf{x_d}(k) = \left(\mathbb{I}_n - \frac{h}{2}\mathbf{A}(kh)\right)\mathbf{x}(kh) - \frac{h}{2}\mathbf{B}(kh)\mathbf{w}(kh)$ and

$$\mathbf{A_{d\,p}}(\boldsymbol{\Delta}) \approx \mathbb{I}_n + (\mathbf{A}+\boldsymbol{\Delta_A})h + (\mathbf{A}+\boldsymbol{\Delta_A})\frac{h^2}{2} + (\mathbf{A}+\boldsymbol{\Delta_A})^3\frac{h^3}{4}\ . \tag{22}$$

Thus the approximation of $\mathrm{e}^{\mathbf{A}(\boldsymbol{\Delta})h}$ by $\mathbf{A_{d\,p}}(\boldsymbol{\Delta})$ is only a first order approximation if the zoh method is used, whereas it is a second order approximation with the foh and Tustin methods. Note that for the zoh and foh methods, $\underline{\mathbf{A_d}}$, as defined in Eq.(A3a), is equal to the nominal monodromy matrix

($\mathbf{R_a}(\mathbf{\Delta} = 0)$) obtained from Eq.(8) while approximations are made when the Tustin method is used. Therefore if $\mathbf{\Delta_A}$ is assumed to be small, a better approximation with the foh method than the Tustin method can be expected. Indeed, the Taylor expansion (20) is equal to (16) except for a fourth order term in $\mathbf{\Delta_A} h^3/12$. It is also important to underline the crucial influence of n_h on the accuracy of the result. High values of n_h tend to minimize errors with all the methods, but also substantially increase robustness analysis computation time since the number of inputs and outputs of the initial LFT model is multiplied by n_h in the new uncertainty block $\underline{\widetilde{\mathbf{\Delta}}}$.

This Taylor expansion based analysis allows us to recommend the foh method for the discretization of the LFT representation of uncertain systems instead of the more commonly used zoh method. This will be confirmed through the numerical results on the study of the ground resonance phenomenon in section III B.

III. Ground Resonance Parametric Analysis

A. Ground resonance modeling

Figure 2 provides a general diagram of the dynamical system. It represents a simplified helicopter model similar to that used in the earliest research of the ground resonance phenomenon [1].

The fuselage is modeled as a rigid body with mass m_f. $x_f(t)$ and $y_f(t)$ represent the fuselage positions along the longitudinal and lateral directions, respectively. The mechanical impedance between the fuselage and the ground (landing gear) is modeled by two stiffnesses $K_{f\,X}$ and $K_{f\,Y}$ and two damping factors C_X and C_Y acting in the longitudinal and lateral directions. At equilibrium, the fuselage center of mass (point O) coincides with the origin of the inertial reference frame (X_0, Y_0, Z_0).

The rotor head system is comprised of one rigid rotor hub and an assembly of N_b blades. The k-th blade has a mass $m_{b\,k}$, a moment of inertia $I_{z\,b\,k}$ around the z - axis located at its center of mass and an in-plane lead-lag motion defined by $\varphi_k(t)$. The radius of gyration is defined by the length b. Angular spring and viscous damping are considered on each blade hinge (point B). Spring stiffness and viscous damping coefficients are denoted $K_{b\,k}$ and $C_{b\,k}$, respectively.

The origin of the fuselage frame (x, y, z), parallel to the inertial frame, is located at the geometric center of the rotor hub (coincident at point O). The rotor angular velocity is denoted Ω.

The fuselage and rotor head are joined by a rigid shaft while aerodynamic forces on the blades are not taken into account. This assumption is quite realistic since the helicopter is on the ground. Also note that aerodynamic effects can be embedded in the uncertainties on blade hinge damping and stiffness. In the present work, the rotor is composed of $N_b = 4$ blades.

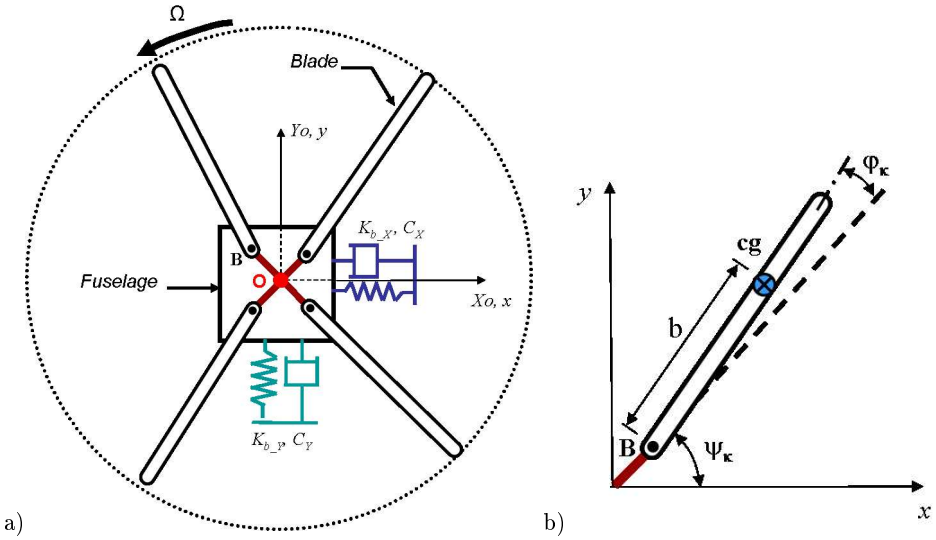

Figure 2: Diagram of the Mechanical System

The position of the k-th blade center of mass, written in the inertial reference frame, is given as:

$$x_{b\,k} = a\cos(\psi_k) + b\cos(\psi_k + \varphi_k(t)) + x_f(t) \tag{23a}$$

$$y_{b\,k} = a\sin(\psi_k) + b\sin(\psi_k + \varphi_k(t)) + y_f(t) \tag{23b}$$

where a is the hinge offset and $\psi_k = \Omega t + \frac{2\pi(k-1)}{N_b}$, $k = 1, \cdots, N_b$.

The expressions of the kinetic energy, the potential energy and the work of dissipative forces are presented separately in Appendix B. By applying Lagrange equations and a first order expansion of trigonometric terms, the linear dynamic model can be derived:

$$\mathbf{M}\,\ddot{\mathbf{q}} + \mathbf{G}\,\dot{\mathbf{q}} + \mathbf{K}\,\mathbf{q} = \mathbf{F_{ext}} \tag{24}$$

where $\mathbf{q}(t) = [\, x_f(t) \;\; y_f(t) \;\; \varphi_1(t) \;\; \varphi_2(t) \;\; \varphi_3(t) \;\; \varphi_4(t) \,]^T$ is the generalized coordinates vector. $\mathbf{M}$,

G and **K** correspond to the mass, damping and stiffness matrices respectively and are described in Eq.25. These matrices are not symmetric due to the presence of periodic terms. $\mathbf{F_{ext}}$ is equal to zero if all the blades have the same inertial and geometrical properties.

$$\mathbf{M}(t) = \begin{bmatrix} 1 & 0 & -r_{m1}\sin(\psi_1) & -r_{m2}\sin(\psi_2) & -r_{m3}\sin(\psi_3) & -r_{m4}\sin(\psi_4) \\ 0 & 1 & r_{m1}\cos(\psi_1) & r_{m2}\cos(\psi_2) & r_{m3}\cos(\psi_3) & r_{m4}\cos(\psi_4) \\ -r_{b1}\sin(\psi_1) & r_{b1}\cos(\psi_1) & 1 & 0 & 0 & 0 \\ -r_{b2}\sin(\psi_2) & r_{b2}\cos(\psi_2) & 0 & 1 & 0 & 0 \\ -r_{b3}\sin(\psi_3) & r_{b3}\cos(\psi_3) & 0 & 0 & 1 & 0 \\ -r_{b4}\sin(\psi_4) & r_{b4}\cos(\psi_4) & 0 & 0 & 0 & 1 \end{bmatrix} \tag{25a}$$

$$\mathbf{G}(t) = \begin{bmatrix} r_{cX} & 0 & -2\Omega r_{m1}\cos(\psi_1) & -2\Omega r_{m2}\cos(\psi_2) & -2\Omega r_{m3}\cos(\psi_3) & -2\Omega r_{m4}\cos(\psi_4) \\ 0 & r_{cY} & -2\Omega r_{m1}\sin(\psi_1) & -2\Omega r_{m2}\sin(\psi_2) & -2\Omega r_{m3}\sin(\psi_3) & -2\Omega r_{m4}\sin(\psi_4) \\ 0 & 0 & r_{c1} & 0 & 0 & 0 \\ 0 & 0 & 0 & r_{c2} & 0 & 0 \\ 0 & 0 & 0 & 0 & r_{c3} & 0 \\ 0 & 0 & 0 & 0 & 0 & r_{c4} \end{bmatrix} \tag{25b}$$

$$\mathbf{K}(t) = \begin{bmatrix} \omega_x^2 & 0 & \Omega^2 r_{m1}\sin(\psi_1) & \Omega^2 r_{m2}\sin(\psi_2) & \Omega^2 r_{m3}\sin(\psi_3) & \Omega^2 r_{m4}\sin(\psi_4) \\ 0 & \omega_y^2 & -\Omega^2 r_{m1}\cos(\psi_1) & -\Omega^2 r_{m2}\cos(\psi_2) & -\Omega^2 r_{m3}\cos(\psi_3) & -\Omega^2 r_{m4}\cos(\psi_4) \\ 0 & 0 & \omega_{b\,1}^2+\Omega^2 r_{a\,1}^2 & 0 & 0 & 0 \\ 0 & 0 & 0 & \omega_{b\,2}^2+\Omega^2 r_{a\,2}^2 & 0 & 0 \\ 0 & 0 & 0 & 0 & \omega_{b\,3}^2+\Omega^2 r_{a\,3}^2 & 0 \\ 0 & 0 & 0 & 0 & 0 & \omega_{b\,4}^2+\Omega^2 r_{a\,4}^2 \end{bmatrix} \tag{25c}$$

$$\mathbf{F_{ext}}(t) = \begin{bmatrix} \sum_{k=1}^{N_b} \Omega^2 r_{m\,k}\left(\frac{a+b}{a}\right)\cos(\psi_k) \\ \sum_{k=1}^{N_b} \Omega^2 r_{m\,k}\left(\frac{a+b}{a}\right)\sin(\psi_k) \\ 0 \\ 0 \\ 0 \\ 0 \end{bmatrix} \tag{25d}$$

where: $r_{m\,k} = \frac{b\,m_{b\,k}}{m_f+\sum_{k=1}^{N_b} m_{b\,k}}$, $r_{b\,k} = \frac{b\,m_{b\,k}}{b^2\,m_{b\,k}+I_{z_{b\,k}}}$, $r_{a\,k}^2 = a\,r_{b\,k}$, $r_{c\,X..Y} = \frac{C_{X..Y}}{m_f+\sum_{k=1}^{N_b} m_{b\,k}}$, $\omega_x^2 = \frac{K_{f\,X}}{m_f+\sum_{k=1}^{N_b} m_{b\,k}}$, $\omega_y^2 = \frac{K_{f\,Y}}{m_f+\sum_{k=1}^{N_b} m_{b\,k}}$, $r_{c\,k} = \frac{C_{b\,k}}{b^2\,m_{b\,k}+I_{z_{b\,k}}}$, $\omega_{b\,k}^2 = \frac{K_{b\,k}}{b^2\,m_{b\,k}+I_{z_{b\,k}}}$, $k = 1, \cdots, N_b$

The aging or failure of mechanical elements comprising the helicopter rotor head, e.g., springs or dampers, has a direct influence on the dynamical behavior of the whole system. Depending on the degradation of these elements, new critical rotating velocities may be reached at which the ground resonance phenomenon will occur. Thus the robustness analysis of helicopters under structured uncertainties is required to predict the smallest perturbation leading the system to instability. The uncertainties introduced on the mechanical model are related to blade hinge stiffnesses $K_{b\,k}$ and damping factors $C_{b\,k}$. The 4 blade hinge stiffnesses are normalized with respect to the in-plane lead-lag cantilevered frequency squared:

$$\omega_{b\,k}^2 = (1+\delta_k)\,\overline{\omega}_{b\,k}^2 \quad (k = 1,\, 2,\, 3,\, 4) \tag{26}$$

where δ_k corresponds to the relative uncertainties related to $\overline{\omega}_{b\,k}^2$ (i.e.: square of the nominal blade resonance frequency).

According to Eq.(1), the LTP model $\mathcal{S}(\boldsymbol{\Delta})$ of the ground resonance phenomenon taking into account uncertainties on the 4 blade hinge stiffnesses takes to form:

$$\mathbf{A}(t) = \begin{bmatrix} \mathbb{O}_{6\times 6} & \mathbb{I}_6 \\ -\mathbf{M}^{-1}(t)\mathbf{K}(t) & -\mathbf{M}^{-1}(t)\mathbf{G}(t) \end{bmatrix}, \quad \mathbf{B}(t) = \begin{bmatrix} \mathbb{O}_{6\times 4} \\ -\mathbf{M}^{-1}(t) \begin{bmatrix} \mathbb{O}_{2\times 4} \\ \\ \mathbb{I}_4 \end{bmatrix} \end{bmatrix} \tag{27}$$

$$\mathbf{C}(t) = \begin{bmatrix} \begin{bmatrix} \mathbb{O}_{4\times 2} & \text{diag}[\overline{\omega}_{b\,1}^2, \overline{\omega}_{b\,2}^2, \overline{\omega}_{b\,3}^2, \overline{\omega}_{b\,4}^2] \end{bmatrix} & \mathbb{O}_{4\times 6} \end{bmatrix}, \quad \mathbf{D}(t) = \mathbb{O}_{4\times 4} \tag{28}$$

$$\boldsymbol{\Delta} = \text{diag}[\delta_1,\, \delta_2,\, \delta_3,\, \delta_4] \tag{29}$$

associated with the state vector $\mathbf{x} = [\mathbf{q}^T \quad \dot{\mathbf{q}}^T]^T$.

The model relative to the 4 blade hinge damping factors is described in section III C, equation (31). The numerical data are summarized in Table 1.

Table 1: **Nominal parameters of a helicopter with identical blades**

Fuselage	
$m_f = 2902.9$ [kg]	
$\omega_x = 6.0\,\pi$ [rad/s]	$\omega_y = 8.0\,\pi$ [rad/s]
$C_X = 5.71\,10^3$ [Ns/m]	$C_Y = 7.62\,10^3$[Ns/m]
Rotor	
$a = 0.2$ [m]	$b = 2.5$ [m]
$m_{b\,k} = 31.9$ [kg]	$\overline{\omega}_{b\,k} = 3.0\,\pi$ [rad/s]
$I_{zb\,1..4} = 259$ [kg m^2]	$C_{b\,1..4} = 432$ [Nms/rad]

B. Validation of the lifting procedure

The objectives of this section are: (i) to validate the lifting procedure presented in section II B by comparison with Floquet analyses for various configurations of the uncertain parameters, and (ii) to select the best discretization method while minimizing the over-sample number n_h in order to obtain a good trade-off between analysis accuracy and CPU-time reduction. The following assumptions are made:

- only the 4-th blade hinge stiffness is considered to be uncertain (i.e.,$\Delta = \text{diag}[0,\, 0,\, 0,\, \delta_4]$),

- the rotor angular velocity is constant: $\Omega = 10\pi\, rad/s$.

The discrete-time lifted model $\underline{\widetilde{\mathcal{M}}}_d(\mathrm{z})$ in Eq.(11) is constructed for three different values of n_h (10, 30 and 100) and the three discretization methods (zoh, foh, Tustin). Then, for each value of the uncertainty δ_4 (from -100% to 100% by steps of 10%), the LFT $\underline{\widetilde{\mathcal{M}}}_d(\mathrm{z}) - \underline{\widetilde{\mathbf{\Delta}}}$ is resolved and compared with the Floquet monodromy matrix $\mathbf{R_a}(\mathrm{diag}[0,0,0,\delta_4])$ computed with $n_h = 100$ (Eq. 8). The comparison index is the highest eigenvalue (or characteristic multiplier) magnitude denoted $\overline{|\lambda_l|}(\delta_4)$ and $\overline{|\lambda_{\mathbf{R_a}}|}(\delta_4)$ for the lifted model and the monodromy matrix, respectively. Note that the nominal angular velocity ($\Omega = 10\pi\, rad/$) leads to a weak stability margin (in terms of characteristic multiplier magnitude), which is quite sensitive to parametric uncertainties. Indeed, the maximal characteristic multiplier magnitude of $\mathbf{R_a}(\mathbb{O}_{4\times4})$ is $\overline{|\lambda_{\mathbf{R_a}}|}(0) = 0.982$. The results for the three discretization methods are presented in Figures 3 to 5 and summarized in Table 2. From these results, it can be concluded that:

- for high values of n_h ($n_h = 100$), the stability analyses obtained with the three methods converge with the Floquet-based prediction,
- for low values of n_h, the stability analysis based on the zoh method is poor,
- the best trade-off between stability-analysis accuracy and the reduction of n_h is obtained with the foh method and $n_h = 30$. This value will be adopted in the next section.

Table 2: **Maximal relative error (%) on the highest characteristic multiplier magnitude with respect to the nominal stability margin:** $\max_{\delta_4}\left(\left|\overline{|\lambda_l|}(\delta_4) - \overline{|\lambda_{\mathbf{R_a}}|}(\delta_4)\right|\right)/(1 - \overline{|\lambda_{\mathbf{R_a}}|}(0))$**.**

n_h	10	30	100
zoh	323	115	35
foh	14.5	1.43	0.49
Tustin	125	14.5	1.49

It can also be concluded that rotor stability is quite robust with respect to variations of single blade stiffness. Instability occurs (i.e. highest characteristic multiplier magnitude greater than 1) only for very low values of δ_4 ($\delta_4 < -90\%$).

Remark III.1 *The CPU-time for computing the lifted model* (11) *on a standard desk-top computer is* 0.39 s, 1.98 s *and* 17.7 s, *respectively for* $n_h = 10$, 30 *and* 100 *(the effect of the discretization method on CPU-time is negligible). The CPU-time for computing the monodromy matrix* (15) *with* $n_h = 100$ *is* 1.26 s.

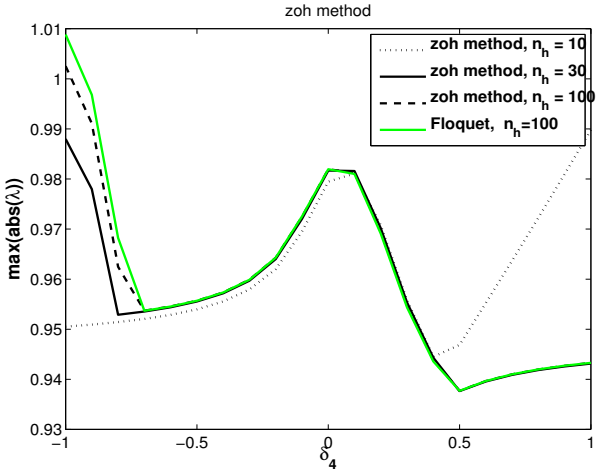

Figure 3: Evolution of the magnitude of the highest characteristic multiplier with respect to δ_4: $\overline{|\lambda_l|}(\delta_4)$, for different values of n_h using zoh method in the lifting procedure, and $\overline{|\lambda_{\mathbf{R_a}}|}(\delta_4)$.

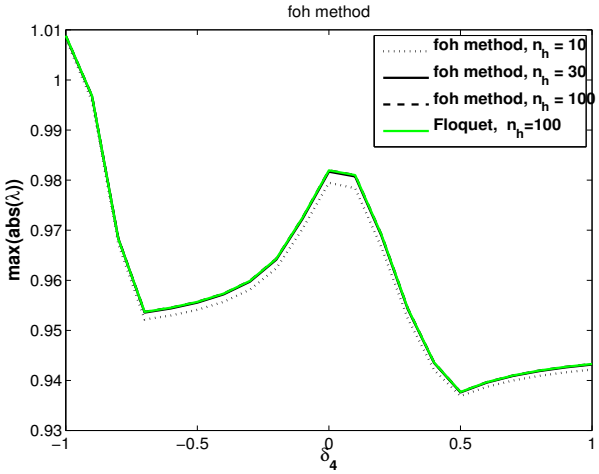

Figure 4: Evolution of the highest magnitude of the characteristic multiplier with respect to δ_4: $\overline{|\lambda_l|}(\delta_4)$, for different values of n_h using foh method in the lifting procedure, and $\overline{|\lambda_{\mathbf{R_a}}|}(\delta_4)$.

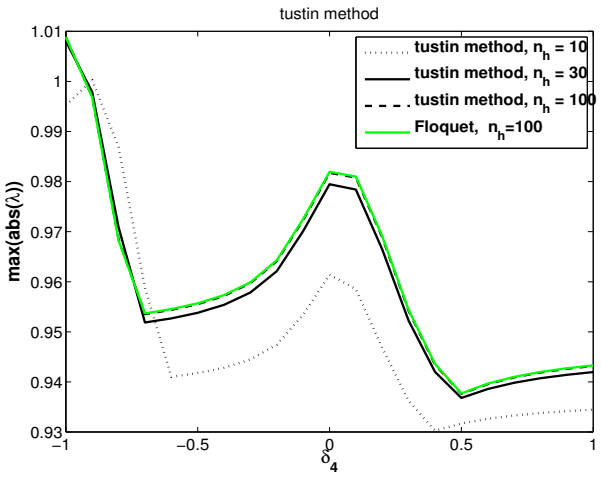

Figure 5: Evolution of the highest characteristic multiplier magnitude with respect to δ_4: $\overline{|\lambda_l|}(\delta_4)$, for different values of n_h using the Tustin method in the lifting procedure, and $\overline{|\lambda_{\mathbf{R_a}}|}(\delta_4)$.

C. μ-analysis of ground resonance stability

In this section, all blade hinge stiffnesses are considered to be uncertain and independent. The μ-analysis toolbox [2] can be directly applied to the continuous-time lifted model $\widetilde{\mathcal{M}}_c(s)$ in Eq.(12). The structure of the uncertainty block $\underline{\widetilde{\mathbf{\Delta}}}_{120\times120}$ is therefore 4 real independent parameters repeated 30 times each. At each frequency ω, the μ-analysis computes an upper bound $\bar{\mu}(\omega)$ and a lower bound $\underline{\mu}(\omega)$ of the structured singular value μ. The μ-upper bound provides a guarantee of robust stability, i.e.

$$\mathcal{S}(\mathbf{\Delta}) \text{ is stable} \quad \forall\, \delta_i \;/\; |\delta_i| \leq \frac{1}{\max_\omega \bar{\mu}(\omega)}\,, \quad i = 1,\, 2,\, 3,\, 4$$

while the μ-lower bound provides the worst parametric configuration $\mathbf{\Delta}_{worst}(\omega)$ [34].

For the nominal rotor angular velocity $\Omega = 10\pi$ rad/s, the μ-upper and lower bounds provided by the Skew Mu Toolbox are plotted in Figure 6. It can be concluded that $\max_\omega \bar{\mu}(\omega) = 12$ (i.e. the parametric robustness margin is 8.3 %) and $\max_\omega \underline{\mu}(\omega) \approx \max_\omega \bar{\mu}(\omega)$ (i.e. this margin is not at all conservative). The μ-analysis tools also provide the critical frequency $\omega^c_{worst} = 23.7\, rad/s$, the frequency of the instability that occurs when $\mathbf{\Delta} = \mathbf{\Delta}_{worst}$. The parametric configuration at ω^c_{worst}

---

[2] Ferreres, G. and Biannic, J.-M., "The Skew Mu Toolbox", `http://www.onera.fr/staff-en/jean-marc-biannic/`.

is

$$\boldsymbol{\Delta}_{worst} = \mathrm{diag}[0.085,\ 0.085,\ 0.085,\ 0.085]\,.$$

It is now possible to compute the monodromy matrix $\mathbf{R_a}(\boldsymbol{\Delta}_{worst})$ (Eq.15) to validate the μ-analysis result and the representativeness of the lifted model. The 12 eigenvalues (characteristic multipliers) of $\mathbf{R_a}(\boldsymbol{\Delta}_{worst})$ associated with the 6 "monodromic modes" are given in Table 3. Mode # 2 is unstable with a magnitude very close to one.

Table 3: **Characteristic multipliers of matrix $\mathbf{R_a}(\boldsymbol{\Delta}_{worst})$.**

Mode	Characteristic multipliers	Magnitude
# 1	$0.1836 \pm 0.7602\,j$	0.7821
# 2	$-0.6981 \pm 0.7164\,j$	1.0003
# 3	$-0.5907 \pm 0.4742\,j$	0.7575
# 4	$-0.7088 \pm 0.5466\,j$	0.8951
# 5	$-0.5962 \pm 0.6876\,j$	0.9101
# 6	$-0.5962 \pm 0.6876\,j$	0.9101

Although rotor stability is quite robust regarding uncertainty on a single blade hinge stiffness (see section III B), robustness to uncertainties on all four blades is quite poor. Our analysis showed that the worst case configuration corresponds to a rotor with identical blades. An interesting observation regarding this analysis is that no dissimilar blades configurations are worse than $\boldsymbol{\Delta}_{worst}$ from a stability point of view. This point is confirmed by further analysis considering uncertainties on 2 adjacent blades, 2 opposing blades and 3 blades (see Table 4 for a summary of μ-analysis results). Once again, considering Figure 4, the best stability margin in term of the highest characteristic multiplier magnitude is obtained for $\delta_4 = 0.5$. The stability robustness analysis for an asymmetric rotor where $\overline{\omega}^2_{b\,4} \leftarrow 1.5\,\overline{\omega}^2_{b\,4}$ leads to the following results:

$$\max_{\omega} \bar{\mu}(\omega) = 8.11, \quad \boldsymbol{\Delta}_{worst} = \mathrm{diag}[0.1312,\ 0.1312,\ 0.1312,\ -0.1312]\,. \tag{30}$$

This analysis confirms that the parametric robustness margin is better for a rotor with dissimilar blade hinges. Thus to improve ground resonance stability it is possible to imagine a mechanism

mounted on a single blade hinge and only operated on the ground in order to create asymmetry in the rotor's properties. Of course, this analyze concerns only the ground resonance phenomenon and any conclusion regarding the advantages of a rotor with dissimilar blade hinges cannot be extended to behavior during flight.

Other analyses were performed for various rotor angular rates Ω (from 1 to 10 Hz). In all cases, the worst case configuration corresponds to a symmetric configuration (i.e.: $\delta_1 = \delta_2 = \delta_3 = \delta_4 = \delta$). Assuming that δ is repeated for the 4 blades, the stability analysis can be simplified (1 uncertain parameter repeated 120 times) and it is possible to plot the stability domain according to δ for various rotor angular rates Ω. This stability domain in the $\Omega - \delta$ plane is shown in Figure 7 and confirms that the stability margin of the nominal configuration ($\Omega = 10\pi\,(\mathrm{rad/s})$, $\delta = 0$) is very weak. It is also noteworthy that if the stability analysis is restricted to symmetric uncertainties, the discrete-time lifted model $\widetilde{\underline{\mathcal{M}}}_d(\mathrm{z})$ can be used directly to plot the evolution of characteristic multipliers as a function of δ in the z-plane using a basic root locus [27]. This plot is presented in Figure 8 in the case $\Omega = 10\pi\,(\mathrm{rad/s})$. Instability occurs for $\delta = 0.085$ at frequency

$$\omega^d_{worst} = 0.74 \times \text{ (half sampling frequency)} = 0.74 \times 5\pi\,\mathrm{rad/s} = 11.5\,\mathrm{rad/s}\ .$$

ω^d_{worst} is linked to ω^c_{worst} by the well-known discrete-time to continuous-time frequency warping of the Tustin transform [27]:

$$\omega^d_{worst} = \frac{2}{T}\mathrm{atan}\left(\frac{T}{2}\omega^c_{worst}\right) \quad \text{with } T = 2\pi/\Omega\ .$$

A possible physical justification of the worst-case configuration can be formulated: for a rotor with identical blade hinges, it is easy to check in Table 3 that modes # 5 and 6 are identical. This multiple-"monodromic" mode may be more significant in the kinematic energy exchange between the rotor and the fuselage than single modes. In other words, the dissymmetry in the rotor breaks this multiple mode and leads to 6 single modes associated with 6 different frequencies and lower modal participation factors. This result must be confirmed by further analyses and confronted with an arbitrary number N_b of blades (an odd number for instance).

Remark III.2 *The CPU-time to compute the lifted model (with $n_h = 30$) and μ-upper bound is*

Table 4: **μ-analysis results for uncertainties on 1 blade, 2 adjacent blades, 2 opposite blades, 3 blades or 4 blades at $\Omega = 5\,Hz$.**

Case	$\max_\omega \bar{\mu}(\omega)$	$\boldsymbol{\Delta}_{worst}$
1 blade	1.1	-0.9
2 adjacent blades	1.41	diag[-0.71, -0.71]
2 opposite blades	1.31	diag[-0.78, -0.78]
3 blades	6.2	diag[0.17, 0.17, 0.17]
4 blades	12	diag[0.085, 0.085, 0.085, 0.085]

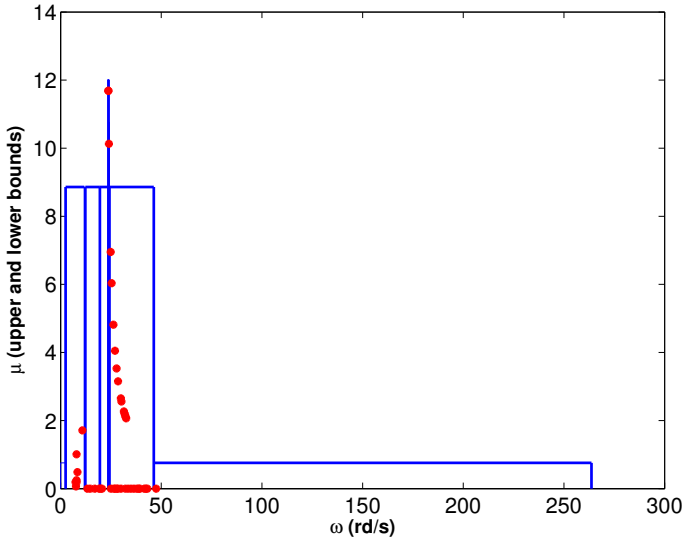

Figure 6: μ upper bound (line) and lower bound ($\bullet$ marks) - robustness stability analysis with respect to uncertainties on the 4 blade hinge stiffnesses at $\Omega = 5\,Hz$.

equal to 8.3 s. *The CPU-time to compute the μ-lower bound on a gridding with 51 frequencies around ω^c_{worst} is equal to* 35 s. *Thus it is possible to use such tools interactively in the MATLAB® environment, which is quite convenient during the design stage. By way of comparison, the CPU-time to compute the monodromy matrix on a parametric space gridding with 20 points per parameter is* 2×10^5 s.

Analyses were also performed to evaluate robustness with respect to the hinge damping factors (parameters $r_{c\,k},\ k = 1, \cdots, N_b$ in Eq. (25a)) which are certainly also very sensitive to aging effects.

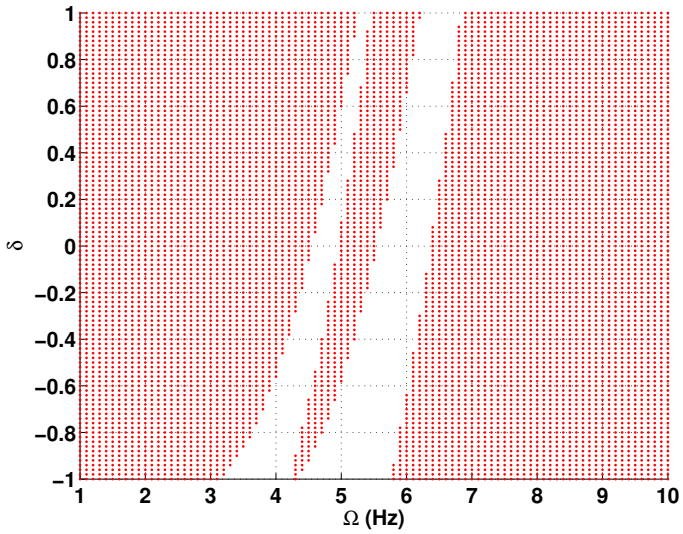

Figure 7: Rotor stability domain (dotted area) according to angular rate Ω and an identical uncertainty δ on the 4 blade hinge stiffnesses.

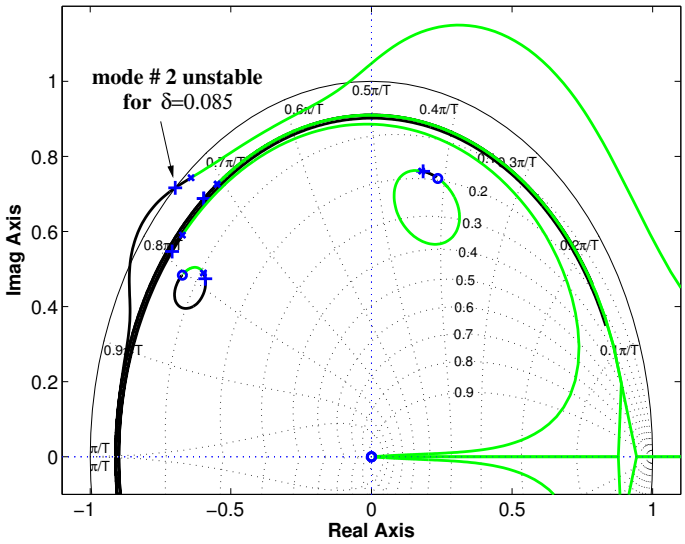

Figure 8: Characteristic multiplier loci in the z-plane according to an identical uncertainty $\delta > 0$ (black) or $\delta < 0$ (grey) on the 4 blade hinge stiffnesses at $\Omega = 5\,Hz$.

The procedure is exactly the same, the main difference is the output matrix Eq. (28) of the initial LTP model which becomes:

$$\mathbf{C}(t) = [\mathbb{O}_{4\times 6} \quad [\mathbb{O}_{4\times 2} \quad \text{diag}\,[\overline{r}_{c\,1}, \overline{r}_{c\,2}, \overline{r}_{c\,3}, \overline{r}_{c\,4}]]] \tag{31}$$

where $\overline{r}_{ck}$ are the parameter nominal values. The μ-analyses provides the following results:

$$\max_{\omega} \bar{\mu}(\omega) = 5.28, \quad \mathbf{\Delta}_{worst} = \text{diag}[-0.198,\ -0.198,\ -0.198,\ -0.198]\ . \tag{32}$$

Once again, the worst case corresponds to a symmetric reduction of all damping factors.

IV. Conclusions

A procedure that combines Floquet theory and the Lifting technique to convert the uncertain linear time periodic (LTP) system into an uncertain linear time-invariant (LTI) lifted system makes it possible to use μ-analysis to determine the smallest perturbation in helicopter blade properties having the worst case effect on rotor stability.

Three discretization methods were compared in order to reduce the complexity (and hence the CPU time) of the lifted model and minimize discretization errors. The conclusion is that the first order hold method gives significantly better results than the more commonly used zero-order hold method.

By taking into account uncertainties on the four blade hinge stiffnesses and damping factors, the μ-analysis shows that the worst case parametric configuration corresponds to a symmetric perturbation for all blade hinges. Thus stability analysis methods restricted to symmetric rotors like the Coleman method are still relevant. Nevertheless, tools are now available to perform further analyses and verify whether this result can be extended to other rotor configurations (for example a rotor system with an odd number of blades). Such tools save significant CPU-time in comparison with a pure Floquet analysis combined with a parametric space exploration.

V. References

[1] Coleman, R. and Feingold, A., "Theory of Self-Excited Mechanical Oscillations of Helicopter Rotors with Hinged Blades," Tech. Rep. Report 1351, NACA Technical Note 3844, 1957.

[2] Bir, G., "Multi-Blade Coordinate Transformation and its Application to Wind Turbine Analysis," *Proc. AIAA/ASME Wind Energy Symp*, No. NREL/CP-500-42553, Reno, Nevada, January 7-10 2008.

[3] Donham, R., Cardinale, S., and Sachs, I., "Ground and Air Resonance Characteristics of a Soft In-Plane Rigid-Rotor System," *Journal of the American Helicopter Society*, Vol. 14, 1969, pp. 33.

[4] Hodges, D., "An Aeromechanical Stability Analysis for Bearingless Rotor Helicopters," *Journal of the American Helicopter Society*, Vol. 24, 1979, pp. 2.

[5] Byers, L. and Gandhi, F., "Embedded Absorbers for Helicopter Rotor Lag Damping," *Journal of Sound and Vibration*, Vol. 325, No. 4-5, 2009, pp. 705 – 721.

[6] Ganiev, R. and Pavlov, I., "The Theory of Ground Resonance of Helicopters," *International Applied Mechanics*, Vol. 9, No. 5, 1973, pp. 505–510.

[7] Wang, J. and Chopra, I., "Dynamics of Helicopters in Ground Resonance with and without Blade Dissimilarities," *AIAA Dynamics Specialists Conference, Dallas, TX*, AIAA, 1992, pp. 273–291.

[8] Arcara, P., Bittanti, S., and Lovera, M., "Periodic Control of Helicopter Rotors for Attenuation of Vibrations in Forward Flight," Vol. 8, No. 6, 2000, pp. 883–894.

[9] Bittanti, S. and Cuzzola, F. A., "Periodic Active Control of Vibrations in Helicopter: a Gain-Scheduled Approach," *Control Engineering Practice*, Vol. 10, 2002, pp. 1043–1057.

[10] Hammond, C., "An Application of Floquet Theory to Prediction of Mechanical Instability," *Journal of the American Helicopter Society*, Vol. 19, 1974, pp. 14.

[11] Skjoldan, P. and Hansen, M., "On the Similarity of the Coleman and Lyapunov-Floquet Transformations for Modal Analysis of Bladed Rotor Structures," *Journal of Sound and Vibration*, Vol. 327, No. 3-5, 2009, pp. 424–439.

[12] Balas, G., Doyle, J., Glover, K., Packard, A., and Smith, R., *μ-Analysis and Synthesis Toolbox: for Use with MATLAB, User's Guide, Version 3*, The MathWorks, Inc, 2001.

[13] Kalender, S. and Flashner, H., "Control Design and Robustness Analysis of Linear Time-Periodic Systems," *Journal of Computational and Nonlinear Dynamics*, Vol. 3, No. 4, 2008, pp. 041003–1 – 041003–10.

[14] Tongue, B. and Flowers, G., "Non-linear Rotorcraft Analysis," *International Journal of Non-Linear Mechanics*, Vol. 23, No. 3, 1988, pp. 189–203.

[15] Flowers, G. and Tongue, B., "Nonlinear Rotorcraft Analysis Using Symbolic Manipulation," *Applied Mathematical Modelling*, Vol. 12, No. 2, 1988, pp. 154–160.

[16] Flowers, G. and Tongue, B., "Experimental Study of the Effects of Nonlinearities on Ground Resonance," *Journal of Guidance, Control, and Dynamics*, Vol. 13, No. 4, 1990, pp. 725–731.

[17] Flowers, G. and Tongue, B., "Chaotic Dynamical Behavior in a Simplified Rotor Blade Lag Model," *Journal of Sound and Vibration*, Vol. 156, No. 1, 1992, pp. 17–26.

[18] Kunz, D. L., "Nonlinear Analysis of Helicopter Ground Resonance," *Nonlinear Analysis: real world applications*, Vol. 3, 2002, pp. 383–395.

[19] Farges, C., Peaucelle, D., and anf J. Daafouz, D. A., "Robust H_2 Performance Analysis and Synthesis of Linear Polytopic Discrete-Time Periodic Systems via LMIs," *Systems and Control Letters*, Vol. 56, 2007, pp. 159 – 166.

[20] Masarati, P., Muscarello, V., and Quaranta, G., "Robust Aeroservoelastic Stability of Helicopters: Application to Air/Ground Resonance," *Proceedings of the AHS 67th Annual Forum*, Curran Associates, Inc, Virginia Beach, VA, 3-5 May 2011, pp. 1191–1201.

[21] Verdult, V., Lovera, M., and Verhaegen, M., "Identification of Linear Parameter-Varying State-Space Models with Application to Helicopter Rotor Dynamics," *International Journal of Control*, Vol. 77, No. 13, 2004, pp. 1149–1159.

[22] Kim, J., Bates, D., and Postlethwaite, I., "Robustness Analysis of Linear Periodic Time-Varying Systems Subject to Structured Uncertainty," *Systems & Control Letters*, Vol. 55, No. 9, 2006, pp. 719–725.

[23] Rabenasolo, B., El Moudni, A., and Richard, J., "Robust Stability for Linear Periodic Systems under Structured Uncertainties," *Systems Analysis Modelling Simulation*, Vol. 16, No. 2, 1994, pp. 123–139.

[24] Kim, J., Bates, D., Postlethwaite, I., Ma, L., and Iglesias, P., "Robustness Analysis of Biochemical Networks Using μ-Analysis and Hybrid Optimisation," *44th IEEE Conference on Decision and Control and 2005 European Control Conference.*, IEEE, Seville (Spain), Dec. 2005, pp. 6234 – 6239.

[25] Ma, L. and Iglesias, P., "Robustness Analysis of a Self-Oscillating Molecular Network in Dictyostelium Discoideum," *Proceedings of the 41st IEEE Conference on Decision and Control*, Vol. 3, IEEE, Las Vegas NV, 2002, pp. 2538–2543.

[26] Ma, L. and Iglesias, P., "Quantifying Robustness of Biochemical Network Models," *BMC Bioinformatics*, Vol. 3, No. 1, 2002, pp. 38.

[27] Franklin, G., Powell, D., and Workman, M., *Digital Control of Dynamic Systems (3rd Edition)*, Prentice Hall, 1997.

[28] Hoagg, J., Lacy, S., Erwin, R., and Bernstein, D., "First-Order-Hold Sampling of Positive Real Systems and Subspace Identification of Positive Real Models," *Proceedings of the American Control Conference*, Vol. 1, IEEE, Boston MA, 2004, pp. 861–866.

[29] Gökçek, C., "Stability Analysis of Periodically Switched Linear Systems Using Floquet Theory," *Mathematical Problems in Engineering*, Vol. 1, No. 2004, 2004, pp. 1–10.

[30] Bittanti, S. and Colaneri, P., *Periodic Systems: Filtering and Control*, Springer, 2009, pp. 81-108.

[31] Imbert, N., "Robustness Analysis of a Launcher Attitude Controller via μ-Analysis," *Proc. of the 15th IFAC Symposium on Automatic Control in Aerospace, Bologna, Italy*, IFAC, September 2001, pp. 481–486.

[32] Tóth, R., Heuberger, P. S. C., and den Hof, P. M. J. V., "On the Discretization of LPV state-space representations," *IET Control Theory & Applications*, Vol. 4, No. 10, 2010, pp. 2082–2096.

[33] Toth, R., Lovera, M., Heuberger, P. S. C., Corno, M., and Van den Hof, P. M. J., "On the Discretization of Linear Fractional Representations of LPV Systems," *IEEE Transactions on Control Systems Technology*, Vol. 20, No. 6, November 2012, pp. 1473 – 1489.

[34] Ferreres, G., *A Practical Approach to Robustness Analysis with Aeronautical Applications*, Kluwer Academics/Plenum Press, 1999, pp. 63-80.

[35] Colaneri, P., Celi, R., and Bittanti, S., "Constant-Coefficient Representations of Periodic-Coefficient Discrete Linear Systems," *Proceedings of the AHS 4th Decennium Specialist Conference on Aeromechanics*, Curran Associates, Inc., San Francisco, CA, Jan. 2004.

Appendix

Appendix A: LIFTING PROCEDURE

The lifting procedure, as described in [22, 35], is summarized here for the reader's convenience. The state-space matrices of the discrete-time lifted model are expressed directly from the state-space matrices provided by the selected discretization method (Eqs.(17) to (21)) and do not involve the transition matrix.

From Eq.(9), let us define the "packed" output and input vectors

$$\underline{\mathbf{w_d}}(k) = \left[\mathbf{w_d^T}(k)\ \mathbf{w_d^T}(k+1)\ \ldots\ \mathbf{w_d^T}(k+n_h-1)\right]^{\mathbf{T}} \tag{A1a}$$

$$\underline{\mathbf{z_d}}(k) = \left[\mathbf{z_d^T}(k)\ \mathbf{z_d^T}(k+1)\ \ldots\ \mathbf{z_d^T}(k+n_h-1)\right]^{\mathbf{T}} \tag{A1b}$$

Then, the integration over one period of system in Eq.(9) leads to the discrete-time lifted system

$$\begin{cases} \mathbf{x_d}(k+n_h) &= \underline{\mathbf{A_d}}\,\mathbf{x_d}(k) + \underline{\mathbf{B_d}}\,\underline{\mathbf{w_d}}(k) \\ \underline{\mathbf{z_d}}(k) &= \underline{\mathbf{C_d}}\,\mathbf{x_d}(k) + \underline{\mathbf{D_d}}\,\underline{\mathbf{w_d}}(k) \\ \text{with} \quad \underline{\mathbf{w_d}}(k) &= \underline{\mathbf{\Delta}}\,\underline{\mathbf{z_d}}(k) \end{cases} \tag{A2}$$

where

$$\underline{\mathbf{A_d}} = \mathbf{\Phi}_0^{n_h-1} \tag{A3a}$$

$$\mathbf{\Phi}_l^u = \prod_{q=l}^{u} \mathbf{A_d}(k+q) = \mathbf{A_d}(k+u)\mathbf{A_d}(k+u-1)\dots\mathbf{A_d}(k+l) \quad \text{if } u \geq l, \tag{A3b}$$

$$\mathbf{\Phi}_l^u = \mathbb{I}_n \quad \text{otherwise.} \tag{A3c}$$

$$\underline{\mathbf{B_d}} = \begin{bmatrix} \mathbf{\Phi}_1^{n_h-1}\mathbf{B_d}(k) & \mathbf{\Phi}_2^{n_h-1}\mathbf{B_d}(k+1) & \dots & \mathbf{\Phi}_{n_h-1}^{n_h-1}\mathbf{B_d}(k+n_h-2) & \mathbf{B_d}(k+n_h-1) \end{bmatrix} \tag{A3d}$$

$$\underline{\mathbf{C_d}} = \begin{bmatrix} \mathbf{C_d}(k) \\ \mathbf{C_d}(k+1)\mathbf{\Phi}_0^0 \\ \vdots \\ \mathbf{C_d}(k+n_h-1)\mathbf{\Phi}_0^{n_h-2} \end{bmatrix} \tag{A3e}$$

$$\underline{\mathbf{D_d}} = \begin{bmatrix} \mathbf{D_d}(k) & 0 & & \\ \mathbf{C_d}(k+1)\mathbf{B_d}(k) & \mathbf{D_d}(k+1) & & \\ \mathbf{C_d}(k+2)\mathbf{\Phi}_1^1\mathbf{B_d}(k) & \mathbf{C_d}(k+2)\mathbf{B_d}(k+1) & & \\ \vdots & \vdots & & \\ \mathbf{C_d}(k+n_h-1)\mathbf{\Phi}_1^{n_h-2}\mathbf{B_d}(k) & \mathbf{C_d}(k+n_h-1)\mathbf{\Phi}_2^{n_h-2}\mathbf{B_d}(k+1) & & \end{bmatrix}$$
$$\begin{bmatrix} 0 & \cdots & 0 \\ 0 & \cdots & 0 \\ \mathbf{D_d}(k+2) & & 0 \\ \vdots & \ddots & \vdots \\ \mathbf{C_d}(k+n_h-1)\mathbf{\Phi}_3^{n_h-2}\mathbf{B_d}(k+2) & \cdots & \mathbf{D_d}(k+n_h-1) \end{bmatrix} \tag{A3f}$$

The general expression for the lower triangular terms of matrix $\underline{\mathbf{D_d}}$ is

$$\underline{\mathbf{D_d}}(i,j) = \mathbf{C_d}(k+i-1)\mathbf{\Phi}_j^{i-2}\mathbf{B_d}(k+j-1) \quad \forall\, i = 1,\dots,n_h,\ j < i\ .$$

The diagonal matrix $\underline{\mathbf{\Delta}}$ is composed of $\mathbf{\Delta} = \text{diag}[\delta_1, \cdots, \delta_p]$ repeated n_h times

$$\underline{\mathbf{\Delta}} = \text{diag}\left[\mathbf{\Delta},\ \mathbf{\Delta},\ \dots\ \mathbf{\Delta}\right] \tag{A4}$$

Finally, since each δ_i for $i = 1, 2, \dots, p$ appears in each Δ block, the row re-ordering matrix can be defined as $\mathbf{V}$ so that

$$\mathbf{V}\underline{\mathbf{\Delta}} = \underline{\widetilde{\mathbf{\Delta}}}\mathbf{V} \tag{A5}$$

with $\underline{\widetilde{\mathbf{\Delta}}} = \mathrm{diag}\,[\delta_1 \mathbb{I}_{n_h},\, \delta_2 \mathbb{I}_{n_h},\, \ldots\, \delta_p \mathbb{I}_{n_h}]$ and $\mathbf{V^T V} = \mathbb{I}_n$.

Let us define the re-ordered "packed" input and output vectors

$$\underline{\widetilde{\mathbf{w}}_\mathbf{d}}(k) = \mathbf{V}\underline{\mathbf{w_d}}(k) \quad \text{and} \quad \underline{\widetilde{\mathbf{z}}_\mathbf{d}}(k) = \mathbf{V}\underline{\mathbf{z_d}}(k)\ ,$$

then the LFT representation (A2) is transformed into the LFT representation (11).

Appendix B: KINETIC AND POTENTIAL ENERGY AND WORK OF DISSIPATIVE FORCE

The kinetic and potential energy expressions and the work expression of dissipative forces of the dynamical system are presented here for the reader's convenience [1, 10]. They are all written in the inertial reference frame.

- The **kinetic energy** of the whole dynamical system consists of the sum of kinetic energy expression of the fuselage T_{Fus} and rotor head T_{RH} systems:

$$T_{Fus} = \frac{m_f}{2}\left(\dot{x}^2(t) + \dot{y}^2(t)\right) \tag{B1a}$$

$$\begin{aligned} T_{RH} &= \frac{1}{2}\sum_{k=1}^{N_b}\left[I_{z_b\,k}\dot{\varphi}_k^2 + m_{b\,k}\left(\dot{x}_{b\,k}^2 + \dot{y}_{b\,k}^2\right)\right] \\ &= \frac{1}{2}\sum_{k=1}^{N_b} I_{z_b\,k}\dot{\varphi}_k^2 + \frac{1}{2}\,m_{b\,k}\sum_{k=1}^{N_b}\left\{\begin{array}{c} (\dot{x}+\dot{y}) + b^2\dot{\varphi}_k^2 + 2b^2\Omega\dot{\varphi}_k + b^2\Omega^2\left(a^2+b^2\right) \\ 2\,a\,b\cos(\varphi_k)\left[\Omega^2+\Omega\dot{\varphi}_k\right] + 2a\Omega[-\dot{x}\sin(\psi_k) + \dot{y}\cos(\psi_k)] \\ 2b(\Omega\dot{y}+\dot{y}\dot{\varphi}_k)\cos(\psi_k+\varphi_k) - 2b(\Omega\dot{x}+\dot{x}\dot{\varphi}_k)\sin(\psi_k+\varphi_k) \end{array}\right\} \end{aligned} \tag{B1b}$$

- The **potential energy** of the whole dynamical system consists of the sum of the potential energy of the fuselage, U_{Fus}, and rotor head, U_{RH}, systems:

$$U_{Fus} = \frac{1}{2}\left(K_{f\,X}\,x^2 + K_{f\,Y}\,y^2\right) \tag{B2a}$$

$$U_{RH} = \frac{1}{2}\sum_{k=1}^{N_b} K_{b\,k}\,\varphi_k^2 \tag{B2b}$$

- The **work of dissipative forces** of the whole dynamical system consists of the sum of the work done by dissipative forces acting on the fuselage δF_{Fus} and the rotor head δF_{RH} systems:

$$U_{Fus} = \frac{1}{2}\left(C_{f\,X}\,\dot{x}^2 + C_{f\,Y}\,\dot{y}^2\right) \tag{B3a}$$

$$U_{RH} = \frac{1}{2}\sum_{k=1}^{N_b} C_{b\,k}\,\dot{\varphi}_k^2 \tag{B3b}$$